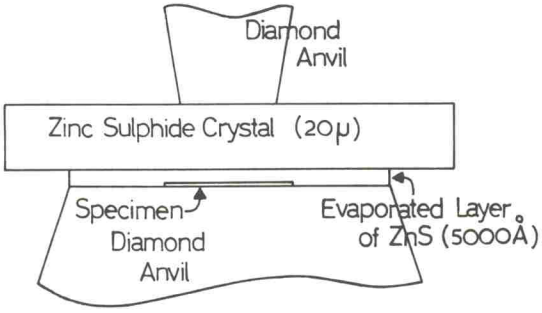

Fig. 2. Schematic representation of the pressure cell. The diagram is not to scale.

The light path was restricted to a small area near the centre of the specimen across which the pressure is essentially constant.

By reducing the area of the crystal under examination the pressure variation can, in principle, be made as small as required. However, signal to noise considerations in the detection system put a lower bound on the area that could be selected. Nevertheless it was shown that in a typical experiment for which $r_s = 0{\cdot}1\, r_0$, where r_s and r_0 are the sampling and anvil radii respectively, the variation in pressure across the specimen was no greater than 1 per cent of the measured pressure. Moreover, the equations of Jackson and Waxman [10] suggest that whenever

$$\frac{2fr_0}{t} \gg 1$$

where f is the coefficient of friction between ZnS and diamond, and t is the ZnS thickness, the pressure at the centre of the anvils is hydrostatic for all types of centrally peaked pressure distributions. Therefore, although we are aware that a solid pressure transmitting medium may produce non-uniform strains, the experimental observations are most probably described by changes in the 'quasi-hydrostatic' pressure experienced by the specimen.

2.2 *Material*

The samples were cleaved from a large natural single crystal of MoS_2 using 'Sellotape'. Suitable specimens can then be transferred to an anvil, by dissolving away the glue with trichloroethylene, and at the same time allowing surface forces to pull the crystal down into intimate contact [11(a)]. The crystals are relatively impure, but there is no observable effect due to these impurities in the region of the excition absorption bands. This has been verified in the case of the analogous material WS_2 by comparing natural and synthetic crystals.

The electrical and photoelectrical properties of these natural crystals, perpendicular to the c-direction, have been investigated by Wieting [12], and the carrier density at room temperature of about $10^{17}\,cm^{-3}$ is similar to the value ($5 \times 10^{16}\,cm^{-3}$) obtained by Fivaz and Mooser [13], for crystals grown by vapour phase transport. Therefore, the major impurities, Al and Si, in the natural crystals make little or no contribution to the electrical properties. Inspection of the effective potential in which excess carriers in a layer lattice move, reveals the explanation of this effect. Within each layer but outside the atomic cores the potential is low and varies slowly. Between the layers, however, the contributions of the different atoms add up to high and fairly wide potential barriers. The carriers therefore become localized within individual layers and thus behave as if moving through a stack of independent lamellae. Moreover, this tendency is accompanied by a strong interaction between the free carriers and the homopolar phonons, polarized at right angles to the layers, which leads to an anomalously strong temperature dependence of mobility [14]. Furthermore, impurities lying within the van der Waal's gap, cannot influence either the concentration or scattering behaviour of the charge carriers, although the existence of electrical polarization in the natural crystals and the absence of this polarization in grown crystals [12] indicates that these impurities are present as polarizable molecules, such as Al_2O_3, SiO_2, or possibly aluminium silicate. However, substitutional impurities within a layer produce

n-type material, in which impurity scattering and extrinsic conduction occur below about 250°K (see Sections 4.3 and 5).

3. BAND STRUCTURE AND EXCITON ASSIGNMENT

3.1 *Bonding considerations*

In the following discussions a single layer model is used for the deduction of the relative positions of the energy bands, since interlayer interactions must produce only small perturbations on the interlayer potential [15].

The hybridisation of the atomic wavefunctions, which is required to give the MoS_2 layer structure has been described by Hultgren [16]. The 4 *d*, 5 *s* and 5 *p* orbitals, outside the core of the Mo atom, are combined to make six equivalent cylindrical bond functions with a trigonal prism configuration, together with two degenerate (*d*/*p* hybridisation) and one non-degenerate (d_{z^2}) non-bonding orbitals. The sulphur atoms at the corners of the prisms, on the other hand, use 3 *p* orbitals in the bonding, so that the orbitals perpendicular to the layers, which are then responsible for the interlayer van der Waal's forces, are saturated 3 *s* subshells. It is now necessary to consider how such hybridised orbitals give rise to a band structure.

It appears that the overlap integral between the atomic levels in the molybdenum and sulphur atoms in MoS_2 is so large that in the solid the outer *s*, *p* and *d* orbitals form filled valence bands and empty conduction bands which are separated by a large energy. Indeed, the energy of formation of MoS_2 is comparable to CdI_2, so that the basic bonding gap is of order 5 eV. This implies that the electronic properties are imparted by electrons in bands formed from the non-bonding orbitals, which have energies that lie within the basic gap. Direct evidence for the existence of such bands comes from electron energy loss experiments in the energy range 0–60 eV, which have recently been made by Liang and Cundy [17].

In Fig. 3 are shown the relative positions of the bands, which follow directly from such considerations. The lower valence bands, labelled X_1, and the upper conduction bands X_1^* correspond to σ and σ^*-bonds between the hybridised *s*, *p* and *d* orbitals of molybdenum, and the *p* orbitals of sulphur respectively. The location of the Fermi level depends on the number of outer electrons per molecule, and in MoS_2 lies between the narrow non-bonding bands, X_2 and X_3. The formation of bands from *d*-functions in this way, is not surprising as the metal–metal distance is only 3·16 Å. Furthermore, the large conductivity in NbS_2, 10^6 times greater than in

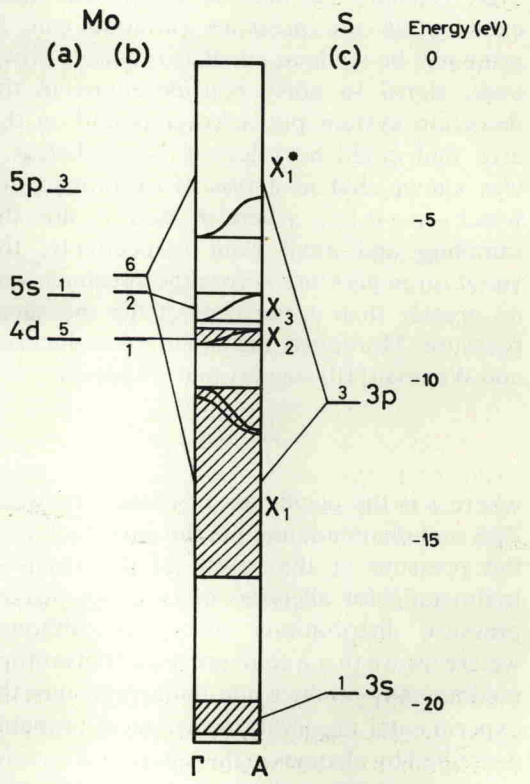

Fig. 3. Suggested electronic band structure of 2H–MoS_2. The energies and degeneracies of the levels in the Mo and S atoms, and in the hybridised Mo atom are shown in columns (a), (c) and (b) respectively. The absolute energy scale is subject to considerable error, but the relative positions of the bands, X_1, X_2, X_3 and X_1^* are correct to a few tenths of an eV.